ACS OMEGA

http://pubs.acs.org/journal/acsodf

Article

Microbial-Catalyzed Baeyer–Villiger Oxidation for 3,4-*seco*-Triterpenoids as Potential HMGB1 Inhibitors

Pingping Shen,[⊥] Jing Zhou,[⊥] Xuewa Jiang, Haixia Ge, Weiwei Wang, Boyang Yu, and Jian Zhang*

Cite This: *ACS Omega* 2022, 7, 18745–18751

Read Online

ACCESS | Metrics & More | Article Recommendations | Supporting Information

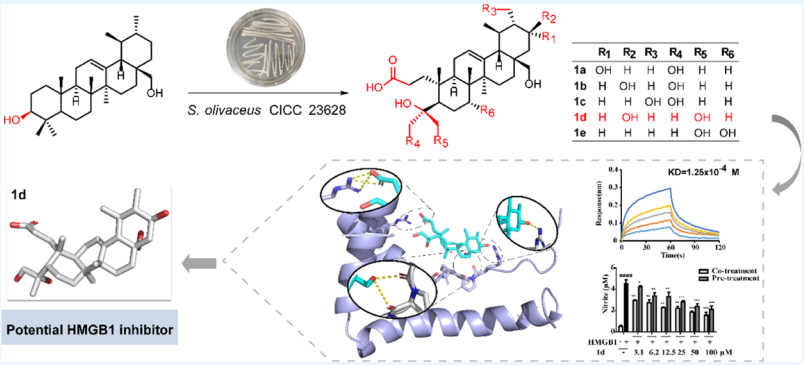

ABSTRACT: Pentacyclic triterpenoids are considered to be the potential HMGB1 inhibitors, but due to the limited number of hydrogen bond donors and the number of rotatable bonds in the rigid skeletons, their further chemical biology research with this target was restricted. To improve these profiles, microbial-catalyzed Baeyer–Villiger oxidation of the primary ursane and oleanane-type triterpenoids including uvaol (**1**), erythrodiol (**2**), oleanolic acid (**3**), and ursolic acid (**4**) was performed by *Streptomyces olivaceus* CICC 23628. As a result, ten new and one known A-ring cleaved metabolites were obtained and the possible biogenetic pathways were also discussed based on the HPLC-MS analysis. Furthermore, the direct interactions between compounds **1d**, **2b**, and HMGB1 were observed by the biolayer interferometry technique. Molecular docking revealed that the newly introduced vicinal diol at C-4, C-24, and the hydroxyl group at C-21 of compound **1d** are crucial for binding with HMGB1. The cellular assay showed that co-treatment of **1d** could significantly block HMGB1-activated nitric oxide release with an IC_{50} value of 9.37 μM on RAW 264.7 cells. Altogether, our research provides some insights into 3,4-*seco*-triterpenes as potential anti-inflammatory candidates for the discovery of novel HMGB1 inhibitors.

1. INTRODUCTION

High mobility group box 1 (HMGB1) is a non-histone chromatin-associated protein, widely distributed in eukaryotic cells.[1] In response to a stimulus such as an infection or a sterile injury, HMGB1 can be passively released or actively secreted to extracellular context as a danger alarmin.[2] Extracellular HMGB1 triggers and sustains the inflammatory response via the receptor for advanced glycation end products (RAGE) or toll-like receptor 4 (TLR4) by recruiting leucocytes and inducing cytokine release. Blocking excessive amounts of extracellular HMGB1 or HMGB1-RAGE/TLR4 interaction has shown great potential in the treatment of arthritis, colitis, sepsis, ischemia–reperfusion, and cancers.[3]

Pentacyclic triterpenoids (**PTs**), a class of plant-derived natural compounds, have attracted extensive attention in the field of chemistry and biology due to their broad pharmacological properties such as hepatoprotective, anti-inflammatory, anti-viral, and anticancer properties.[4,5] Glycyrrhizin, the most abundant **PT** component of licorice, was the first reported natural antagonist of HMGB1 and has been used for decades to treat patients with hepatitis.[6] Oleanolic acid has also been used clinically as a hepatoprotective drug due to its strong anti-inflammatory potential in targeting HMGB1-mediated inflammation.[7,8] Additionally, a series of synthetic and natural **PT** derivatives such as glycyrrhetinic acid,[9,10] carbenoxolone,[11] and maslinic acid[12] were also found to interact with HMGB1 similarly as glycyrrhizin to exert a wide range of beneficial effects. Despite the significant bioactivity and distinctive affinity with HMGB1, the chemical and biological profiles of **PTs** including rigid five-membered heterocycles, low solubility, and poor bioavailability restricted their further applications.[13] To overcome these limitations, the

Received: March 11, 2022
Accepted: May 12, 2022
Published: May 25, 2022

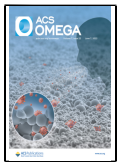

most employed strategy is the addition of oxygen to the skeleton of **PTs** which can not only improve their physicochemical properties (e.g., solubility), but also facilitate the hydrogen bond interactions with their target protein.

In previous studies, we found that A-*seco*-triterpenes could be obtained through biotransformation by *Streptomyces olivaceus* 23628 and the multi-hydroxy groups are critical for their inhibition on HMGB1-induced inflammation.[14] Encouraged by this result, we further explored the general applicability of this novel catalytic system for the discovery of potent HMGB1 inhibitors of **PTs**. A series of A-ring cleaved hydroxy acid isomers was obtained and the possible biotransformation pathways were elucidated by HR-ESI-MS and preliminary genomic analysis. Based on biolayer interferometry (BLI), we evaluated the binding affinity of all compounds to HMGB1 protein. Molecular docking was used to predict the binding characteristics between small molecules and HMGB1. Finally, the anti-inflammatory efficacy of metabolites on HMGB1-induced nitric oxide (NO) release in RAW 264.7 macrophages was determined and the possible structure−activity relationship was also discussed.

2. MATERIALS AND METHODS

2.1. General Experimental Procedures. The CD spectrum was measured on a JASCO 810 spectropolarimeter. NMR spectra were obtained with a Bruker AV-600 and AV-500 spectrometer. Chemical shifts are stated relative to TMS and are expressed as δ (ppm) with coupling constants in Hz. HR-ESI-MS data were acquired using a Micromass AutospecUltima ETOF spectrometer. Preparative HPLC was performed on an Agilent 1100 instrument equipped with an Alltech 3300 ELSD detector and an Ultimate XB-C18 column (250 × 21.2 mm, 5 μm) by eluting with mixtures of acetonitrile and water. TLC was conducted on GF254 silica gel plates (Qingdao Haiyang Chemical Factory, Qingdao, China). Column chromatography experiments were carried out on a Sephadex LH-20 (GE Healthcare) and on silica gel (200−300 mesh, Qingdao Haiyang Chemical Factory, Qingdao, China). Recombinant human HMGB1 was purified in our laboratory. Substrates were purchased from Qingze Pharmacy Co. Ltd., Nanjing, China. *S. olivaceus* CICC 23628 were procured from Prof. John P.N. Rosazza of the University of Iowa, USA.

2.2. Microbial Transformation Procedures. Cultures were grown by a two-stage process in 50 mL of soybean meal glucose medium held in 250 mL culture flasks. The soybean meal glucose medium contained 20 glucose, 5 soybean meal, 5 yeast extract, 5 NaCl, and 5 K_2HPO_4 in distilled water (in g/L) and was adjusted to a pH of 7.0 before being autoclaved at 121 °C for 20 min. Cultures were incubated with shaking at 180 rpm at 28 °C. A 10% inoculum derived from 24 h old stage I cultures was used to initiate stage II cultures, which were incubated for 24 h before receiving 10 mg of the substrate in 1 mL of ethanol, and incubation was conducted as before.[15]

2.3. Extraction, Isolation, and Purification. Cultures were incubated for 4 days and extracted with an equal volume of EtOAc thrice. The organic solvent layer was evaporated to dryness. The crude extracts of biotransformation of substrates (200 mg) with *S. olivaceus* CICC 23628 were subjected to chromatography on a silica gel column (25.0 g, 15 × 400 mm) and eluted with a stepwise gradient system of CH_2Cl_2/MeOH (100:1−5:1) to provide different fractions. Like fraction was separated by preparative HPLC (12 mL/min, acetonitrile in water) using a UV detector at 210 nm. The product yield is the ratio of the number of moles of the product obtained to those of substrates consumed. The culture of oleanolic acid incubated with *S. olivaceus* CICC 23628 was collected at four different points in time at 1, 6, 12, and 24 h. The crude extract was analyzed by HR-ESI-MS and HPLC-MS.

S. olivaceus CICC 23628 stored in our laboratory was genome sequenced for further bioinformatics analysis. We next performed a search in the predicted genome using previously described Type I BVMO specific sequence motifs (Rossmann fold GxGxx[GA] and the Type I BVMOs fingerprints [AG]GxWxxxx[FY]P[GM]xxxD and FxGxxxHxxxW[PD]). The scan was carried out using a tool FIMO from MEME Suite 5.3.3 with a false discovery rate lower than 1×10^{-4} (q value, estimated by FIMO using the Benjamini−Hochberg technique).[16] Two putative BVMOs in the genome of *S. olivaceus* CICC 23628 were found,[17] and one of them shared 38.49% sequence identity with PockeMO from *Thermothelomyces thermophilus* ATCC 42464.

2.4. X-ray Crystallographic Analysis. Colorless needle crystals of the methyl esterification derivative of **2** were obtained from MeOH/H_2O (10:1). Crystal data were obtained on a Bruker APEX-II CCD with Ga Kα radiation (λ = 1.34139 Å) at 190(2) K. The structure was solved by direct methods using SHELXT 2014/5 and expanded using different Fourier techniques, refined with SHELXL-2017/1. Crystal data: $C_{31}H_{52}O_6$ (M = 520.72); monoclinic crystal (0.200 × 0.160 × 0.150 mm^3); space group C2; unit cell dimensions a = 26.6755(9) Å, b = 6.9678(2) Å, c = 17.6779(6) Å, V = 2848.38(16) Å^3, α = 90°, β = 119.9020(10)°, and γ = 90°; Z = 4; ρ_{calc} = 1.214 mg/cm^3; μ = 0.416 mm^{-1}; 26203 reflections measured; 5228 unique (R_{int} = 0.0447) which were used in all calculations; final R indices ($I > 2\sigma(I)$) gave R_1 = 0.0480, wR_2 = 0.1402; R indices (all data) gave R_1 = 0.0535, wR_2 = 0.1466; and absolute structure parameter = −0.04 (11). Crystallographic data for the methyl esterification derivative of **1a** have been deposited in the Cambridge Crystallographic Data Centre (deposition number: CDCC 2046279).

2.5. Binding Assays. The binding capacity between the compounds and HMGB1 was determined by BLI using an Octet Red 96 instrument (ForteBio Inc.). Biosensors were hydrated for 10 min before running an assay. HMGB1 with a His-tag (SinoBiological, 10326-H08H) was first loaded onto the Ni-NTA biosensor for 600 s at a concentration of 100 μg/mL. The association and disassociation steps were detected in a running buffer with a constant 1% DMSO concentration. Compounds were allowed to associate with the biosensor surface and then to disassociate with the biosensor in the PBS buffer. All the assays were performed on a Corning 96-well black plate and data were collected at 25 °C with 1000 rpm rotary shaking. Compounds isolated and glycyrrhizin (the positive control) were tested ranging from 16.12 to 500 μM in duplicates. The biosensor without loading-expressed protein was used as a negative control. The equilibrium dissociation constant (KD) values for HMGB1 were calculated using the software FortéBio Octet RED96 according to the global fits of the k_{on} and k_{off} values.

2.6. Molecular Modeling. The molecular docking was performed to generate the possible binding mode between compounds and HMGB1 by using the Glide program in Maestro 11.8 (China Pharmaceutical University). The spatial structure of HMGB1 (PDB: 1HMF) was fetched from the PDB website as a target for docking. The protein was prepared

https://doi.org/10.1021/acsomega.2c01352
ACS Omega 2022, 7, 18745−18751

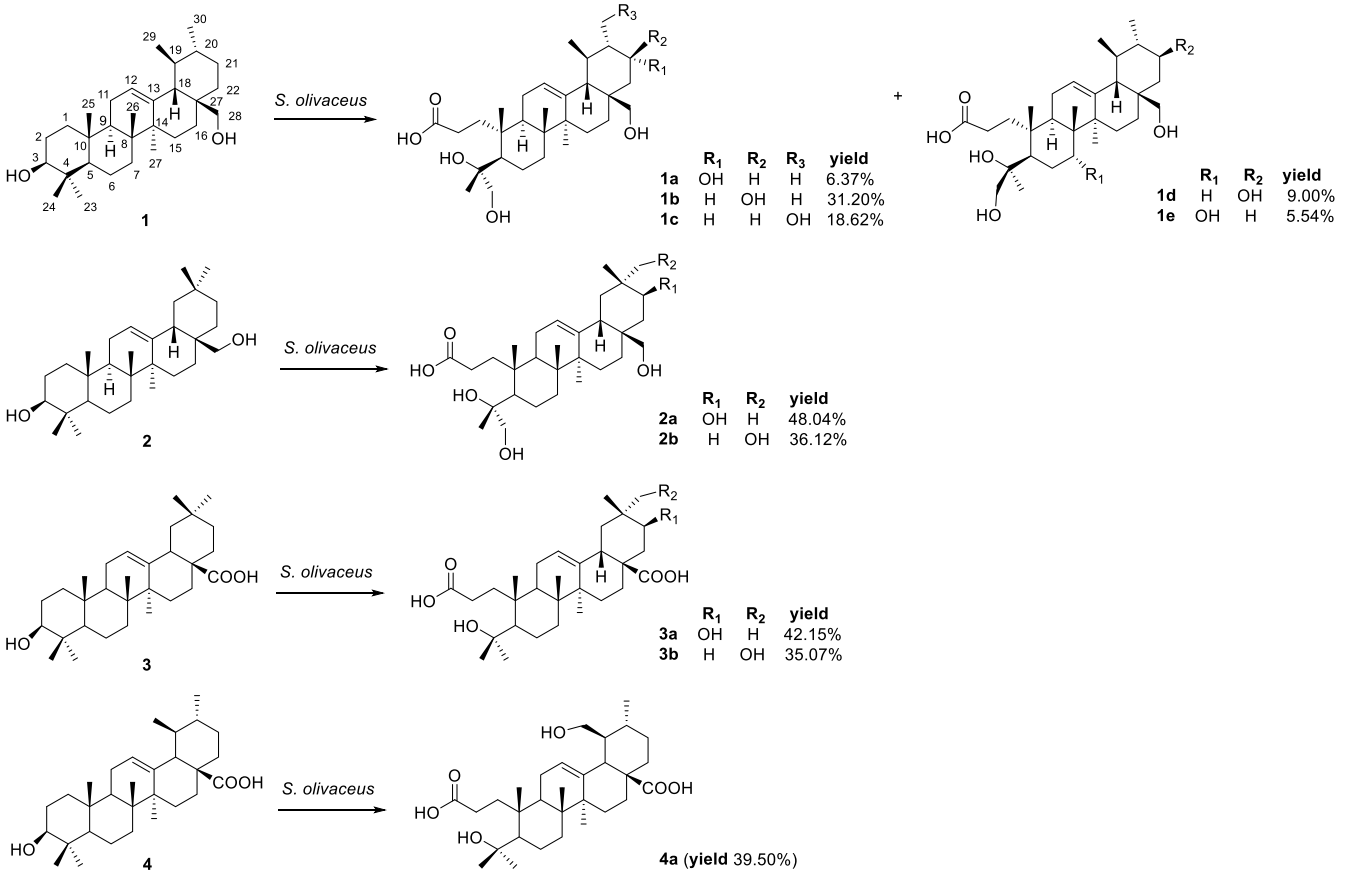

Figure 1. Biotransformation of **1**−**4** by *S. olivaceus* CICC 23628.

by the Protein Preparation Wizard module in Maestro. The ligands were optimized by the LigPrep module to generate all different protonation states and all stereoisomers. Extra precision (XP) mode was used to perform molecular docking. The final pose for the ligand was selected according to the Glide scoring function and visual inspection for further analysis.

2.7. Inhibitory Activity against NO Production Induced by HMGB1. The RAW 264.7 cell lines were cultivated in DMEM added with 10% fetal bovine serum with penicillin G (100 units/mL) and streptomycin (100 μg/mL) at 37 °C in an atmosphere of 5% CO_2 and 95% humidity. The adherent cells were added to a 96-well culture plate at a density of 1 × 10^5 cells per well and incubated with the test compounds for 1 h before the presence or absence of HMGB1 (0.5 μg/mL). Following 24 h of treatment, the nitrite concentration in culture supernatants was measured by the Griess reagent kit (Beyotime, China). Besides, HMGB1 was co-incubated with the compound **1d** at various concentrations for 15 min in vitro and then added to the cell and the supernatant was detected after 24 h. The absorbances at 540 nm were read by a microplate reader (Tecan Trading AG, Switzerland). The cell viability was determined by the MTT assay.

3. RESULTS AND DISCUSSION

3.1. Preparation of 3,4-*seco*-Triterpenes by *S. olivaceus* CICC 23628. After 96 h fermentation of **1**−**4** with *S. olivaceus* CICC 23628 under a mild condition, the microbial multiple selective oxidation reactions were achieved for direct synthesis of 11 A-ring cleaved hydroxy acids **1a**−**4a** (Figure 1). The structures were elucidated by HR-ESI-MS and 1D/2D NMR spectroscopy, induced circular dichroism, and X-ray crystallographic analysis (Figure 2) listed in the Supporting Information. The 3,4-*seco*-ursane triterpenoids accompanied by the adjacent diol moiety obtained in this work were the first occurrence, which makes them a distinctive member of triterpenoids. In general, these multi-step sequential reactions gave an overall yield of about 40−80% based on the starting material in a one-pot process.

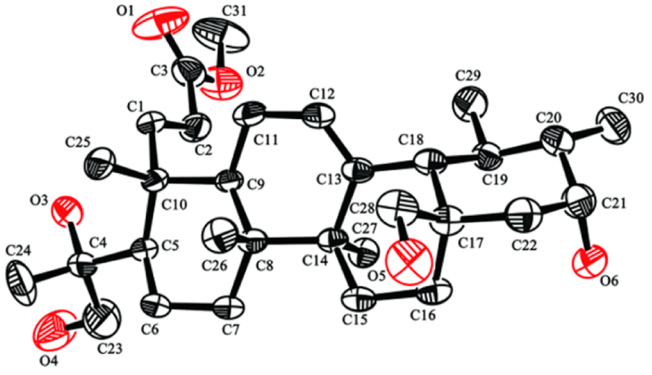

Figure 2. X-ray crystallographic analysis of the methyl esterification product of **1a**.

3.2. Elucidation of the Possible Pathways in the Biotransformation of Oleanolic Acid. To get a better understanding of the reactions coupled in the biotransforma-

https://doi.org/10.1021/acsomega.2c01352
ACS Omega 2022, 7, 18745−18751

Scheme 1. Presumed Multi-Reaction Pathways by HPLC-MS in the $[M - H]^-$ Ion Mode

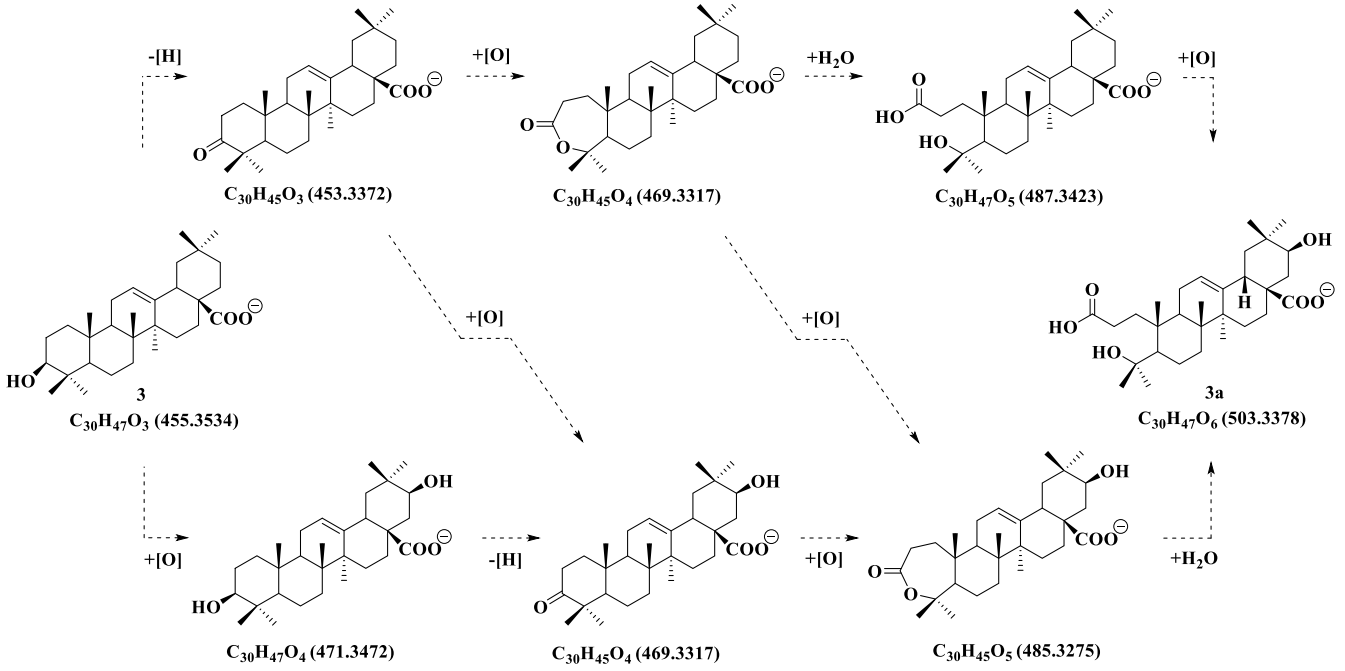

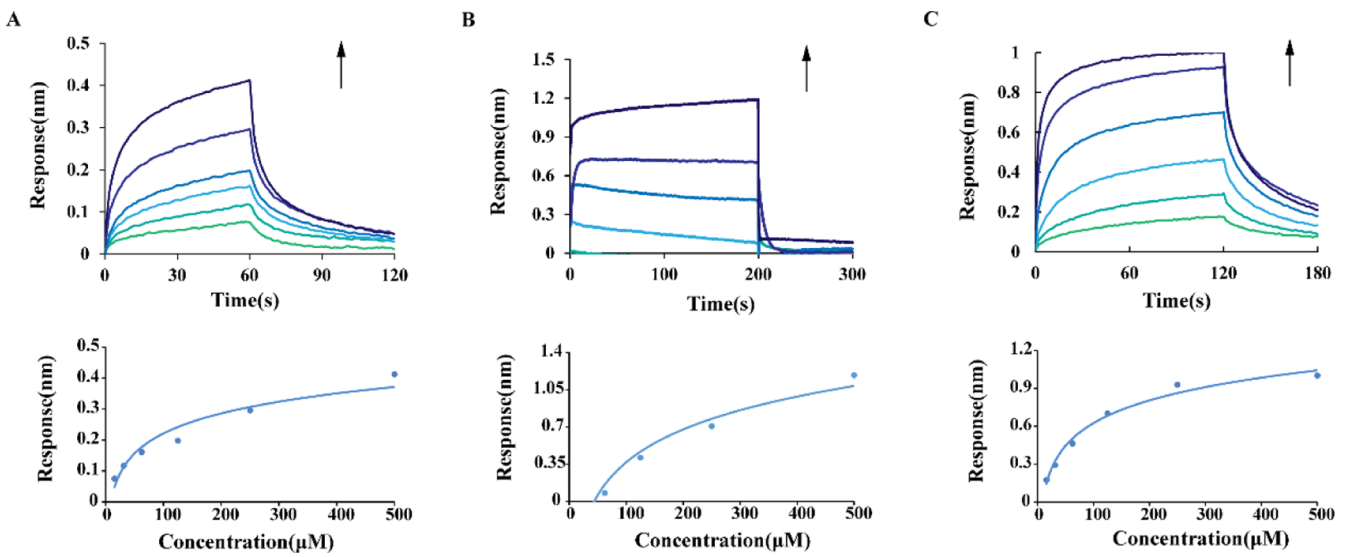

Figure 3. BLI sensorgrams and steady-state affinity analysis of HMGB1 binding to compounds **1d** (A), **2b** (B), and glycyrrhizin (C) to HMGB1.

tion process, we further analyzed the crude extract of oleanolic acid fermentation broth via HR-ESI-MS in the negative ion mode. To our surprise, the $[M - H]^-$ ion peak at m/z 503.3393 (calcd for $C_{30}H_{47}O_6$, 503.3378) was detected at the first hour, indicating that the final A-ring cleavage products were generated very fast. At the same time, the $[M - H]^-$ ion peak at m/z 453.3372 (calcd for $C_{30}H_{45}O_3$, 453.3374) was observed. The 2 amu mass decrease relative to oleanolic acid suggested that the dehydrogenation process was involved. Besides, a new $[M - H]^-$ ion peak occurred at m/z 469.3317 (calcd for $C_{30}H_{45}O_4$, 469.3323), indicating a 16 amu increase relative to the product of dehydrogenation. According to the changes in molecular weight, the peak at m/z 469.3317 ($C_{30}H_{45}O_4$) refers to either the lactone intermediate generated by B−V oxidation or the product of dehydrogenation coupled with hydroxylation of oleanolic acid. In addition, the peak at m/z 487.3423 (calcd for $C_{30}H_{47}O_5$, 487.3429) was also detected. The increment of 18 amu mass compared to the lactone intermediate reminded us that hydrolysis of the lactone ring may occur. The resulting intramolecular ring-opening intermediate was further hydroxylated to form the final product with a 16 amu increase in molecular weight. From the above recorded results, we can infer that the dehydrogenation of chiral secondary alcohol of C-3, B−V oxidation, hydrolysis, and hydroxylation was involved in the catalytic process.

After a careful analysis, additional two negative ion peaks were observed at m/z 471.3472 (calcd for $C_{30}H_{47}O_4$, 471.3480) and 485.3275 (calcd for $C_{30}H_{45}O_5$, 485.3272), suggesting a 16 and 32 amu increase relative to oleanolic acid, respectively. It means that the hydroxylation might occur before B−V serial oxidation (dehydrogenation, B−V oxidation,

https://doi.org/10.1021/acsomega.2c01352
ACS Omega 2022, 7, 18745−18751

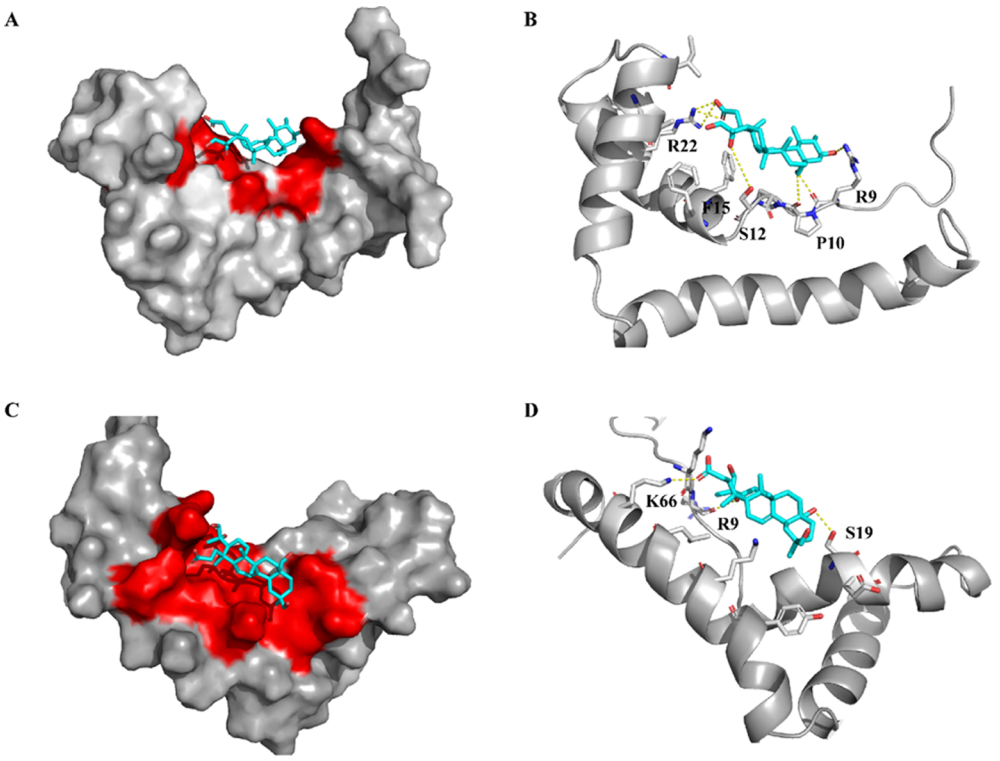

Figure 4. Potential binding models of HMGB1 and compound **1d** (A,B) and **2b** (C,D).

and hydrolysis). In fact, in the complex reaction system, these two types of reactions should be independent, which may occur alternately or simultaneously. With these efforts, the presumed multi-pathway networks identified are presented in Scheme 1, which provides some insights into the tailoring reactions of the biogenetic pathway of 3,4-*seco*-triterpenoids in Nature.

The regio- and stereo-selective hydroxylation at C-7 and C-21 and an angular methyl group at C-29/30 of the triterpene skeleton was achieved in this work. Besides, it showed high stereoselectivity between triterpenic acid and the corresponding diol. When triterpene diol was used as substrates, the hydroxylation at C-23/24 coupled with the serial B−V oxidation gave a chiral vic-diol unit on the A-ring inaccessible by chemical pathways. When the C-28 position is replaced by the carboxyl group, the hydroxylation at C-23/24 did not occur, but the difference in the C-28 functional group did not block the B−V series biocatalytic reactions of the A-ring. It is consistent with our previous report, which indicated the powerful catalytic potential of the BVMO system rooted in *S. olivaceus* CICC 23628. To further validate this, genomic sequencing and bioinformatics analysis were performed. The results revealed the presence of two putative BVMOs in *S. olivaceus* CICC 23628. One of them displayed a 38.49% sequence identity with previously described PockeMO (NCBI Accession: XP_003661890), which has been reported as Type I BVMO to perform oxidations on the A-ring of steroids.[18] However, other enzymes involved in multi-step cascade reactions are under exploration in our laboratory and this work will be published in the future.

3.3. BLI Tests on the Direct Interaction of Metabolites with HMGB1. To evaluate the direct binding capacity of all the compounds with HMGB1, we performed the BLI assay, which is identified as one of the most common ways to determine the binding affinity of ligand−protein interactions.[19] His-tagged HMGB1 was immobilized on NTA biosensor and incubated with serially diluted test compounds. The binding of small molecules to HMGB1 on the biosensor increases the optical thickness at the biosensor tip and results in a wavelength shift, which in turn is measured in real time as a shift in the interference pattern. As shown in Figure 3, a dose-dependent binding manner was observed according to the association and dissociation curves for compounds **1d**, **2b**, and glycyrrhizin. The KD values of compounds **1d**, **2b**, and glycyrrhizin were calculated as 1.25×10^{-4}, 4.90×10^{-3}, and 1.85×10^{-4} M, respectively. Among them, the affinity constant of glycyrrhizin−HMGB1 interaction is about 185 μM, which is close to that reported in the literature (150 μM).[3,6] Thus, it can be concluded that compound **1d** could bind to HMGB1 with a moderate binding ability, which is stronger than that of glycyrrhizin under the same conditions. Compound **2b** exerted a quite feeble binding ability (KD > 1 mM), whereas no obvious shift was observed in the association curve upon the addition of other compounds (Table S2). Considering the above results, we found that the vicinal diol formed after the A-ring cleavage and the newly added hydroxyl group on the E-ring was crucial to the binding of HMGB1.

3.4. Molecular Docking. The HMGB1 structure contains two distinct DNA-binding functional domains (A-box and B-box) and an acid tail. B-box is the main active domain of HMGB1, which is released into the extracellular region to stimulate the secretion of cytokines.[20] A-box can compete with B-box for the binding sites on receptors such as TLR4/MD2, leading to a decrease in inflammation. Two independent and noncooperative binding sites in the A-box and B-box regions have been reported.[6] To get deep insights into the possible binding modes between hit compounds **1d**, **2b**, and HMGB1

https://doi.org/10.1021/acsomega.2c01352
ACS Omega 2022, 7, 18745−18751

(PDB ID: 1HMF), molecular docking was performed using the Glide program in Maestro 11.8.

The stereoviews of the docked poses with the lowest energy are depicted in Figure 4. As is shown, compounds **1d** and **2b** can be bounded to the shallow concave surface of HMGB1. From **4A** and **4B**, the new carboxyl group of compound **1d** formed multiple stable hydrogen bonds with R22, and the hydroxyl group at C-4 and C-28 can form three stable hydrogen bonds with S12 and P10, respectively. Besides, the hydrogen bond between the new C-21 hydroxyl group on the E-ring of compound **1d** and R9 was observed with a bond length of 2.9 Å, which was crucial in maintaining the stability of the compound **1d**-HMGB1 complex. In **4C** and **4D**, the carboxyl group and the C-4 hydroxyl group on compound **2b** can form two stable hydrogen bonds with K66 and R9 of the active pocket of HMGB1. At the same time, the hydroxyl group at the C-28 position can also form a hydrogen bond with the S19 with a bond length of 2.9 Å. According to the results of molecular docking, two flexible chains formed after the opening of A-ring greatly facilitated the hydrogen bonding interactions with the target protein HMGB1, which was consistent with our hypothesis. Except for the difference in the absolute configuration of vicinal diol on the A-ring, the position and configuration of the newly added hydroxyl group on the E-ring also were crucial for the formation of the complex, especially the C-21 hydroxyl group in compound **1d**. When the position of hydroxyl group was changed to C-29, the binding capacity with HMGB1 of compound **2b** decreased obviously, as demonstrated by BLI analysis.

3.6. Inhibitory Effects on HMGB1-Induced NO Production. In this study, the anti-inflammatory activities of all the compounds were evaluated against NO production on HMGB1-stimulated RAW 264.7 cells with carbenoxolone as the positive control. As shown in Figure 5, 0.5 μg/mL HMGB1 can stimulate RAW264.7 cells to release excessive NO, which is significantly different from the control group. Pre-treatment with compound **1d** could interfere with HMGB1-elicited NO production in a dose-dependent manner, with an IC_{50} value of 47.21 ± 7.62 μM. However, the other compounds showed no apparent inhibitory effects under essentially identical conditions (Table S3). In addition, the MTT assay indicated that none of the metabolites had obvious cytotoxicity at the tested concentration. To further study the inhibitory behavior, compound **1d** was co-incubated with HMGB1 at various concentrations for 15 min and then added to the cells. The results showed a significant increase in inhibition with the IC_{50} value of 9.37 ± 2.87 μM, even lower than that of carbenoxolone (IC_{50} = 11.42 μM). It can be inferred that the inhibitory effects of compound **1d** can be attributed to its binding property with HMGB1 protein. Our work systematically clarified the influence of the A-ring cleavage of **PTs** on the interaction with HMGB1 and anti-inflammatory activity, guiding the rational design of HMGB1 inhibitor.

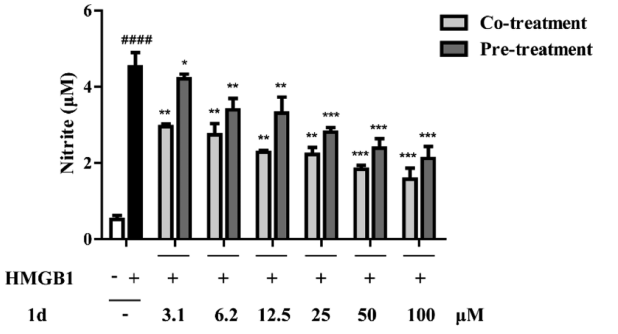

Figure 5. Inhibitory effect of compound **1d** in two different administration modes (pre-treatment or co-treatment with HMGB1) on RAW264.7 cells (the data generated are from 3 replicate experiments. n = 4, values are the mean ± SEM. $^{\#\#\#}P < 0.001$ vs the control group, $^{*}P < 0.05$, $^{**}P < 0.01$, $^{***}P < 0.001$ vs the HMGB1 group).

4. CONCLUSIONS

In conclusion, four primary **PTs** including uvaol, erythrodiol, oleanolic acid, and ursolic acid were selected as substrates for further structural modifications by *S. olivaceus* CICC 23628 to improve their drug-likeness properties. As a result, an array of A-ring cleaved triterpenes were obtained and selective dehydrogenation, B−V oxidation, lactone hydrolysis, and C−H bond activation were involved in the catalytic process. The affinity assay results showed that compound **1d** can directly bind to HMGB1 and exhibit a considerable NO inhibitory effect on HMGB1-induced RAW 264.7 cells. Molecular docking results showed that the active functional groups on the A- and E-rings were critical in maintaining the stability of the compound **1d**-HMGB1 complex. Overall, our findings provide more inspiration for the rapid access of diverse natural *seco*-triterpenes as potential HMGB1 inhibitors.

■ ASSOCIATED CONTENT

Supporting Information

The Supporting Information is available free of charge at https://pubs.acs.org/doi/10.1021/acsomega.2c01352.

Structural identification of compounds **2a−4a**; Table s1: ^{13}C NMR data of **1a-4a**; Table s2: ForteBio Octet Red system assay results and Table s3: NO production of compounds in HMGB1-induced RAW264.7 cells; Figures s1−s79: 1D NMR (^{1}H NMR, ^{13}C NMR), 2D NMR (HSQC, HMBC, and NOESY), HR-ESI-MS data of **1−4a** and CD spectrum; Figure s80: HPLC-MS spectrum for the biotransformation of oleanolic acid (PDF)

X-ray crystallographic analysis data (CIF)

■ AUTHOR INFORMATION

Corresponding Author

Jian Zhang − *State Key Laboratory of Natural Medicines, China Pharmaceutical University, Nanjing 210009, P. R. China; Jiangsu Key Laboratory of TCM Evaluation and Translational Research, China Pharmaceutical University, Nanjing 211198, P. R. China;* orcid.org/0000-0003-3349-0459; Phone: 86-25-86185157; Email: wilsonzhang99@cpu.edu.cn; Fax: 86-25-86185158

Authors

Pingping Shen − *State Key Laboratory of Natural Medicines, China Pharmaceutical University, Nanjing 210009, P. R. China*

Jing Zhou − *State Key Laboratory of Natural Medicines, China Pharmaceutical University, Nanjing 210009, P. R. China*

https://doi.org/10.1021/acsomega.2c01352
ACS Omega 2022, 7, 18745−18751

Xuewa Jiang − *State Key Laboratory of Natural Medicines, China Pharmaceutical University, Nanjing 210009, P. R. China*

Haixia Ge − *School of Life Sciences, Huzhou University, Huzhou 313000, P. R. China;* orcid.org/0000-0003-3087-457X

Weiwei Wang − *Nanjing Hospital of Chinese Medicine Affiliated to Nanjing University of Chinese Medicine, Nanjing 210033, P. R. China*

Boyang Yu − *Jiangsu Key Laboratory of TCM Evaluation and Translational Research, China Pharmaceutical University, Nanjing 211198, P. R. China*

Complete contact information is available at: https://pubs.acs.org/10.1021/acsomega.2c01352

Author Contributions

⊥P.S. and J.Z. contributed equally to this work.

Notes

The authors declare no competing financial interest.

■ ACKNOWLEDGMENTS

This work was supported by the National Nature Science Foundation of China (NSFC no. 21302052) and the "Program for New Century Excellent Talents in University" awarded to J.Z. (NECT-11-0739). Thanks also give to the Postgraduate Research & Practice Innovation Program of Jiangsu Province (SJKY19_0658).

■ REFERENCES

(1) Wang, S.; Zhang, Y. HMGB1 in inflammation and cancer. *J. Hematol. Oncol.* **2020**, *13*, 116.

(2) Yuan, S.; Liu, Z.; Xu, Z.; Liu, J.; Zhang, J. High mobility group box 1 (HMGB1): a pivotal regulator of hematopoietic malignancies. *J. Hematol. Oncol.* **2020**, *13*, 91.

(3) VanPatten, S.; Al-Abed, Y. High Mobility Group Box-1 (HMGb1): Current Wisdom and Advancement as a Potential Drug Target. *J. Med. Chem.* **2018**, *61*, 5093−5107.

(4) Salvador, J. A. R.; Moreira, V. M.; Gonçalves, B. M. F.; Leal, A. S.; Jing, Y. Ursane-type pentacyclic triterpenoids as useful platforms to discover anticancer drugs. *Nat. Prod. Rep.* **2012**, *29*, 1463−1479.

(5) Zhou, M.; Zhang, R.-H.; Wang, M.; Xu, G.-B.; Liao, S.-G. Prodrugs of triterpenoids and their derivatives. *Eur. J. Med. Chem.* **2017**, *131*, 222−236.

(6) Mollica, L.; De Marchis, F.; Spitaleri, A.; Dallacosta, C.; Pennacchini, D.; Zamai, M.; Agresti, A.; Trisciuoglio, L.; Musco, G.; Bianchi, M. E. Glycyrrhizin binds to high-mobility group box 1 protein and inhibits its cytokine activities. *Chem. Biol.* **2007**, *14*, 431−441.

(7) Kawahara, K.; Hashiguchi, T.; Masuda, K.; Saniabadi, A. R.; Kikuchi, K.; Tancharoen, S.; Ito, T.; Miura, N.; Morimoto, Y.; Biswas, K. K.; Nawa, Y.; Meng, X.; Oyama, Y.; Takenouchi, K.; Shrestha, B.; Sameshima, H.; Shimizu, T.; Adachi, T.; Adachi, M.; Maruyama, I. Mechanism of HMGB1 release inhibition from RAW264.7 cells by oleanolic acid in Prunus mume Sieb. et Zucc. *Int. J. Mol. Med.* **2009**, *23*, 615−620.

(8) Kinjo, J.; Okawa, M.; Udayama, M.; Shono, Y.; Hirakawa, T.; Shii, Y.; Nohara, T. Hepatoprotective and hepatotoxic actions of oleanolic acid-type triterpenoidal glucuronides on rat primary hepatocyte cultures. *Chem. Pharm. Bull.* **1999**, *47*, 290−292.

(9) Cavone, L.; Muzzi, M.; Mencucci, R.; Sparatore, B.; Pedrazzi, M.; Moroni, F.; Chiarugi, A. 18β-glycyrrhetic acid inhibits immune activation triggered by HMGB1, a pro-inflammatory protein found in the tear fluid during conjunctivitis and blepharitis. *Ocul. Immunol. Inflamm.* **2011**, *19*, 180−185.

(10) Yamaguchi, H.; Kidachi, Y.; Kidachi, Y.; Kamiie, K.; Noshita, T.; Umetsu, H. Structural insight into the ligand-receptor interaction between glycyrrhetinic acid (GA) and the high-mobility group protein B1 (HMGB1)-DNA complex. *Bioinformation* **2012**, *8*, 1147−1153.

(11) Li, W.; Li, J.; Sama, A. E.; Wang, H. Carbenoxolone blocks endotoxin-induced protein kinase R (PKR) activation and high mobility group box 1 (HMGB1) release. *Mol. Med.* **2013**, *19*, 203−211.

(12) Lee, W.; Lee, H.; Lee, T.; Park, E. K.; Bae, J.-S. Inhibitory functions of maslinic acid, a natural triterpene, on HMGB1-mediated septic responses. *Phytomedicine* **2020**, *69*, 153200.

(13) Kvasnica, M.; Urban, M.; Dickinson, N. J.; Sarek, J. Pentacyclic triterpenoids with nitrogen- and sulfur-containing heterocycles: synthesis and medicinal significance. *Nat. Prod. Rep.* **2015**, *32*, 1303−1330.

(14) Zhu, Y.; Shen, P.; Wang, J.; Jiang, X.; Wang, W.; Raj, R.; Ge, H.; Wang, W.; Yu, B.; Zhang, J. Microbial transformation of pentacyclic triterpenes for anti-inflammatory agents on the HMGB1 stimulated RAW 264.7 cells by Streptomyces olivaceus CICC 23628. *Bioorg. Med. Chem.* **2021**, *52*, 116494.

(15) Zhu, Y.-Y.; Qian, L.-W.; Zhang, J.; Liu, J.-H.; Yu, B.-Y. New approaches to the structural modification of olean-type pentacylic triterpenes via microbial oxidation and glycosylation. *Tetrahedron* **2011**, *67*, 4206−4211.

(16) Grant, C. E.; Bailey, T. L.; Noble, W. S. FIMO: scanning for occurrences of a given motif. *Bioinformatics* **2011**, *27*, 1017−1018.

(17) Gran-Scheuch, A.; Trajkovic, M.; Parra, L.; Fraaije, M. W. Streptomyces leeuwenhoekiiMining the Genome of : Two New Type I Baeyer-Villiger Monooxygenases From Atacama Desert. *Front. Microbiol.* **2018**, *9*, 1609.

(18) Fürst, M. J. L. J.; Savino, S.; Dudek, H. M.; Gómez Castellanos, J. R.; Gutiérrez de Souza, C.; Rovida, S.; Fraaije, M. W.; Mattevi, A. Polycyclic Ketone Monooxygenase from the Thermophilic Fungus Thermothelomyces thermophila: A Structurally Distinct Biocatalyst for Bulky Substrates. *J. Am. Chem. Soc.* **2017**, *139*, 627−630.

(19) Wang, L.; Li, L.; Zhou, Z.-H.; Jiang, Z.-Y.; You, Q.-D.; Xu, X.-L. Structure-based virtual screening and optimization of modulators targeting Hsp90-Cdc37 interaction. *Eur. J. Med. Chem.* **2017**, *136*, 63−73.

(20) Gaskell, H.; Ge, X.; Nieto, N. High-Mobility Group Box-1 and Liver Disease. *Hepatol. Commun.* **2018**, *2*, 1005−1020.